Supporting Information

Anon et al. 10.1073/pnas.1117814109

SI Materials and Methods

Fabrication of Poly-Dimethylsiloxane (PDMS) Pillar Stencil. To pattern gaps in the cell culture, we took advantage of a stencil containing an array of microfabricated pillars. The microfabrication of the stencils was based on a previously described method (1). Briefly, motifs printed on a negative mask were transferred to a silicon wafer by photolithography, followed by a deep reactive ion etching process to obtain holes down to the desired depth. This silicon master was silanized to facilitate the release of the elastomer and allow reusing the master. Then, PDMS (Sylgard 184; Dow-Corning) was poured over the silicon template and cured at 65 °C for approximately 12 h. The stamp of PDMS pillars can be then peeled off from the master.

Gap Patterning. PDMS pillar microstamps were stuck to fibronectin-coated glass-bottom Petri dishes by mild oxygen plasma treatment. Coating was performed by incubating the glass with a solution of fibronectin (Sigma) in PBS at 20 μg/mL for 1 h at 37 °C. The sample was then submerged for 1 h in a 0.2% Pluronics solution (BASF) (vol/vol) in PBS to prevent cell adhesion on the pillar walls. Cells were seeded highly concentrated in a small volume, close to the pillar stamp, to allow an even distribution of the cells between the pillars. After 15 ± 3 h a confluent monolayer was formed, and PDMS stencils were carefully peeled off with tweezers. For the experiments of different cell packing densities, the density of cells at the seeding step was varied according to different densities degrees, but the waiting time before removing the PDMS stencil was kept the same. On the other hand, to create damage-associated gaps, we proceeded with two distinct experimental approaches: (*i*) to gently press the PDMS pillar array against a confluent monolayer in such a way that cells beneath the pillar are killed ("crushed gaps"); and (*ii*) to run the pillar removal assay without previous incubation of the pillars stencil with pluronics in such a way that cells adhere to pillars walls and membranes are scratched upon pillar removal ("ripped gaps").

Cell Damage Assessment. We assessed cell damage by both propidium iodide (Sigma) and FITC-dextran (40 kDa, Sigma) uptake. Propidium iodide labels the nuclei of damaged cells, whereas FITC-dextran is internalized by membrane-disrupted cells.

Cell Culture and Drug Treatments. Madin-Darby canine kidney (MDCK) strain II cells and stable MDCK cell line expressing actin-GFP or lifeact-GFP were used. Cells were cultured in DMEM supplemented with 10% FCS, 100 U/mL penicillin, and 100 μg/mL streptomycin and maintained at 37 °C in a humidified atmosphere with 5% CO_2. For transfected MDCK cells, the selection antibody geneticin was added at 2 μg/mL. α-Catenin knockdown MDCK cells (kindly provided by James W. Nelson, Stanford University) were maintained as the wild-type cells. Pharmacological inhibitors [Y27632 (Calbiochem), ML-7 (Calbiochem), NSC23766 (Calbiochem) and blebbistatin (Sigma)] were added at 25 μM at least 2 h before releasing the PDMS stamp to ensure proper inhibition of the cells under the PDMS stamp.

Video Microscopy and Image Analysis. Live cell imaging was performed in a Nikon or Olympus microscope, enclosed in an incubator to maintain the samples at 37 °C and 5% of CO_2 throughout the experiments. Images were acquired typically every 15 s with Metamorph software. Live cell tracking was accomplished by incubating cells with DAPI at 4 μg/mL in cell culture media for 6 h and thorough rinsing before imaging. Images were analyzed and processed using the software ImageJ.

Immunofluorescence Microscopy. Cells were fixed at different time points upon pillar stencil removal with 4% paraformaldehyde (Sigma) for 30 min, permeabilized with 0.25% Triton X-100 (Sigma) in PBS (vol/vol) for 5 min, and blocked in 1.5% BSA (Sigma) in PBS for 30 min. Staining was performed with primary rabbit antibody against phospho-MLC (Cell Signaling) diluted 1:200 in 2% BSA in PBS and detected with a polyclonal anti-rabbit conjugated with 488 Alexa Fluor (Invitrogen) at 1:100 in PBS. Actin was visualized with Alexa Fluor 564-conjugated phalloidin (Invitrogen) at 1:1,000 in PBS. Fibronectin and laminin were labeled with a primary rabbit antibody against fibronectin (Invitrogen) and a primary mouse antibody for laminin, both at 1:200, and a secondary polyclonal anti-rabbit and anti-mouse (respectively) conjugated with 488 Alexa Fluor (Invitrogen) at 1:300. For adhesions staining, a primary antibody in rabbit for ZO-1 (Zymed, Invitrogen) and a primary antibody in mouse for E-cadherin (BD Transduction) were used at a dilution of 1:1,000 in 1% BSA/PBS and detected with secondary antibodies against mouse and rabbit conjugated with 488 Alexa Fluor (Invitrogen). Samples were mounted in Mowiol and imaged with a Nikon A1R confocal microscope with a 60× or 100× 1.4 N.A. apochromat oil immersion objective lens. When indicated, samples were imaged in epifluorescence with a Deltavision microscope with a 60× 1.4 N.A. apochromat oil immersion objective lens.

Preparation of Substrates of Different Stiffness. Different PDMS stiffness substrates were achieved by mixing PDMS at different cross-linker:base ratios, namely 1:10 for very stiff substrates, comparable to glass coverslips, 1:25, 1:40, and 1:60. At a 1:60 ratio, the substrate remained mainly elastic with a Young's modulus of approximately 20 kPa (2). A small drop of the mixture was placed on top of a glass coverslip, rendering a thin layer of PDMS. PDMS substrate was cured for at least 2 h at 80 °C. The following day it was coated with fibronectin at 20 μg/mL for 1 h at 37 °C and proceeded with the described gap patterning protocol.

1. du Roure O, et al. (2005) Force mapping in epithelial cell migration. *Proc Natl Acad Sci USA* 102:2390–2395.

2. Murrell M, Kamm R, Matsudaira P (2011) Substrate viscosity enhances correlation in epithelial sheet movement. *Biophys J* 101:297–306.

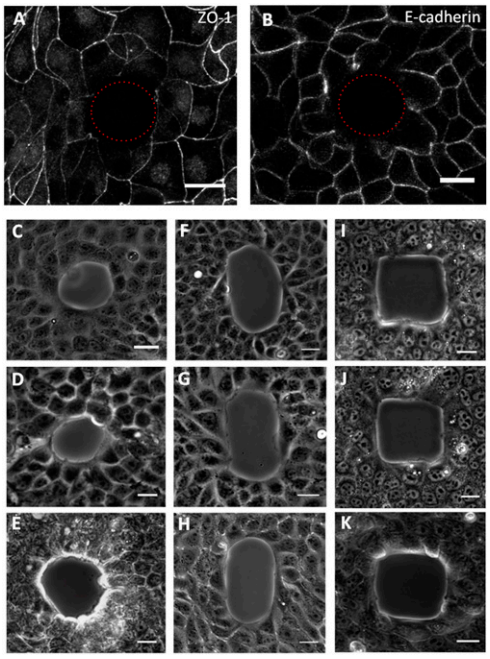

Fig. S1. Initial conditions of cells surrounding the pillars. (*A* and *B*) Immunostaining against adhesion proteins: tight junction protein ZO-1 (*A*) and adherens junction protein cadherin (*B*). Dotted line indicates the pillar position. Note that there are no specific adhesions of the border cells with the pillar. Cells show no preferential alignment along the gap perimeter. (*C–E*) Cells around circular pillar under increasing degree of confluency, from fairly spread (*C*) to highly dense cells (*E*). (*F–H*) Cells are randomly distributed around ellipsoidal gaps. The differential convexity of the gap perimeter does not determine the positioning or alignment of cells at its poles. (*I–K*) Again, the squared shape causes no cornering effect on the distribution of cells, which are evenly positioned. (Scale bars, 20 μm.)

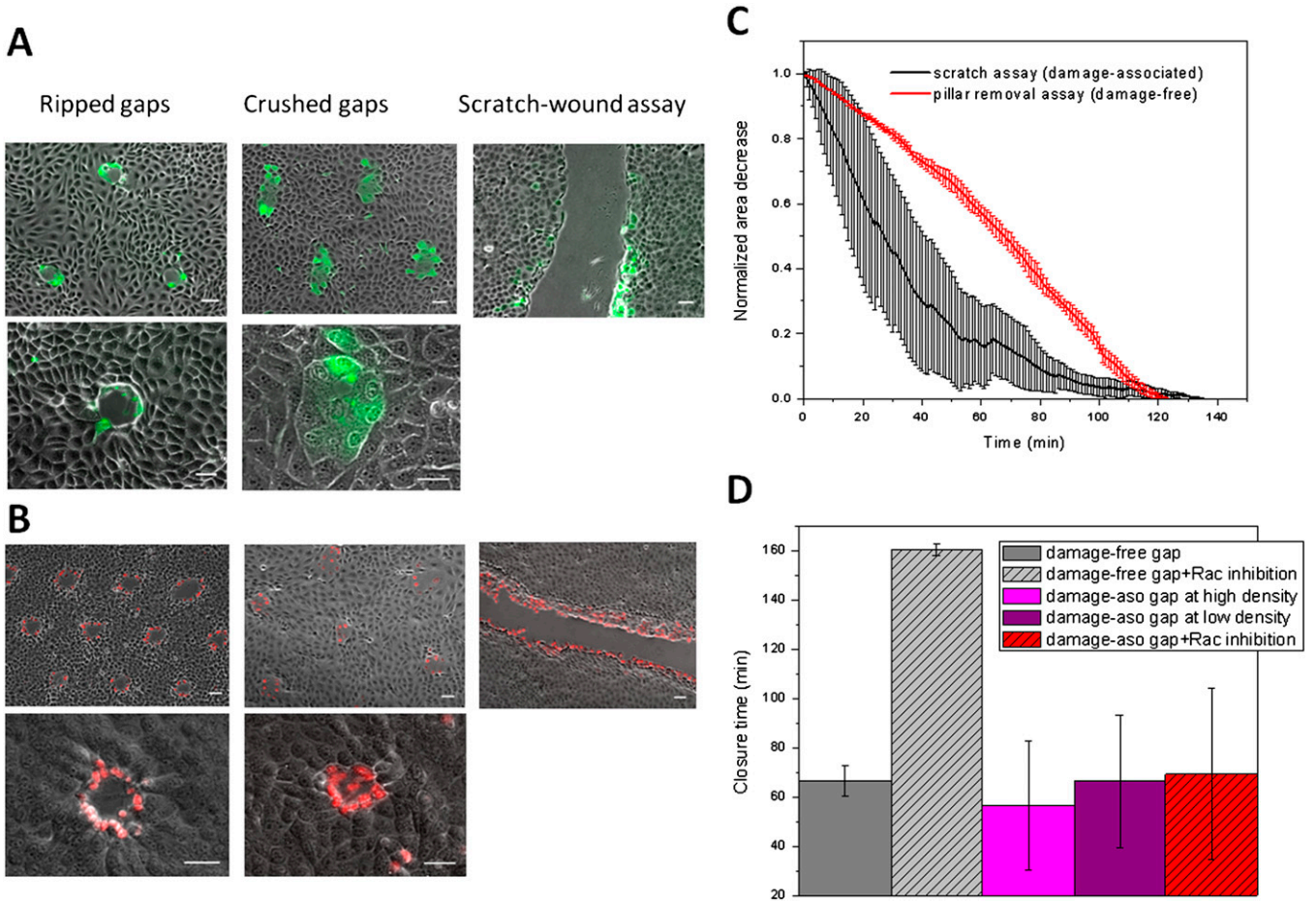

Fig. S2. Characterization of damage-associated "wound" closure experiments. (*A* and *B*) Assessment of cell damage/death in damage-associated gaps by FITC-dextran incorporation (*A*) and propidium iodide (*B*). Crushed gaps result from pressing the pillar array against a confluent monolayer, and ripped gaps are produced by the pillar removal assay without pluronic treatment. In contrast with our damage-free method, both strategies resulted in extensive cell death around the gaps. (Scale bars, 20 μm.) (*C*) Decrease of area over time of the damage-free gaps (created with the pillar removal assay) (red line) vs. the damage-associated gaps (black line). The area has been normalized by the initial area to homogenize the different measurements. (*D*) Closure time of the damage-free gaps in control conditions and under Rac inhibition (gray columns) with respect to damage-associated gaps under low- or high-density conditions and with Rac inhibition (purples and red).

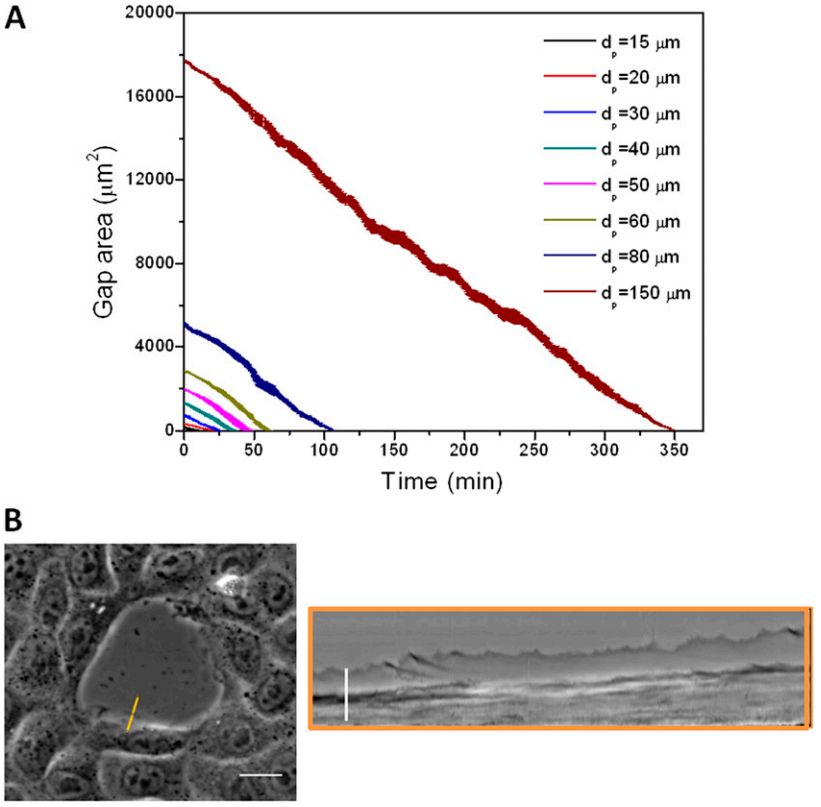

Fig. S3. (*A*) Gap area decrease with time, for different pillar sizes used for creating the gaps, ranging from 15 to 150 μm in diameter. (*B*) Kymograph corresponding to the orange line of the time-lapse snapshot in the left. Frame rate was one frame every 2 s. (Scale bar, 20 μm, *Left*, and 3 μm, *Right*.)

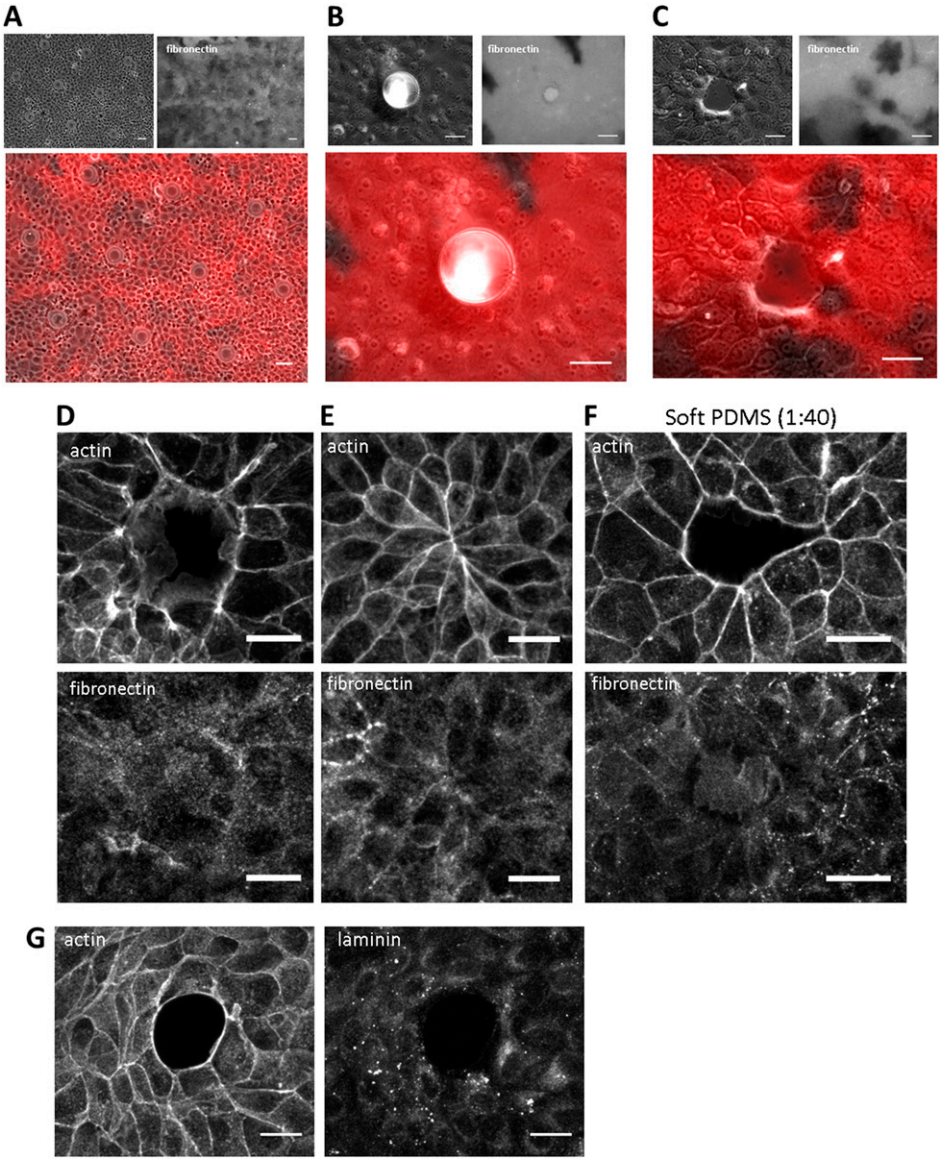

Fig. S4. Extracellular matrix assembly beneath cell culture. We have tested fibronectin location by two approaches: using fluorescently labeled fibronectin to coat the substrate (*A*–*C*) and immunostaining fibronectin to observe fibronectin secretion and reorganization by cells (*D*–*F*). (*A*) Pillars stencil between the epithelial culture on glass at low magnification. (*B*) In a close-up it can be appreciated that fibronectin is present beneath PDMS pillar. (*C*) Removal of the stencil does not tear the fibronectin beneath. (*D*) Fibronectin and actin staining after 30 min of pillar removal and (*E*) at the closure time (65 min after pillar removal). (*F*) Fibronectin deposition on soft PDMS substrates at 1:40 cross-linking ratio is not altered. (*G*) Immunostaining for visualizing laminin assembly: laminin is not present in the gap area, whereas it is in the area covered by cells. (Scale bars, 20 μm.)

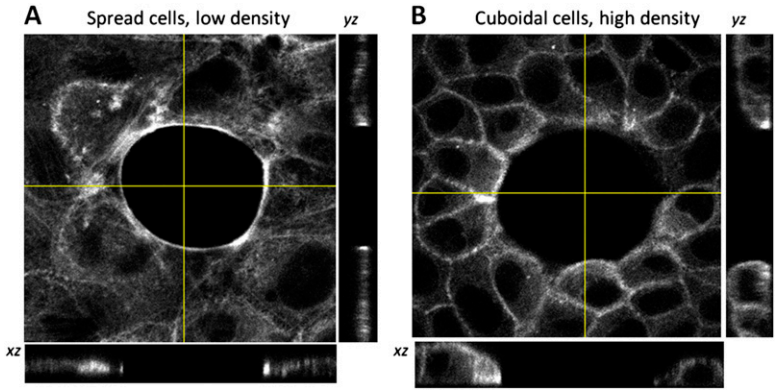

Fig. S5. Effect of cell density on cell monolayer thickness. Central images are the mid-plane of a z-stack, and bottom and right images are orthogonal projections of the stacks on the yellow lines. (*A*) Right upon reaching confluency, cells are highly spread and thus flat. (*B*) As cell density under the pillar stencil increases, cells become smaller and taller. In highly packed cultures, the thickness of the layer is greater than in sparse epithelia. As can be observed in the *x*–*z* and *y*–*z* orthogonal projections, the lateral membrane in dense cultures is larger.

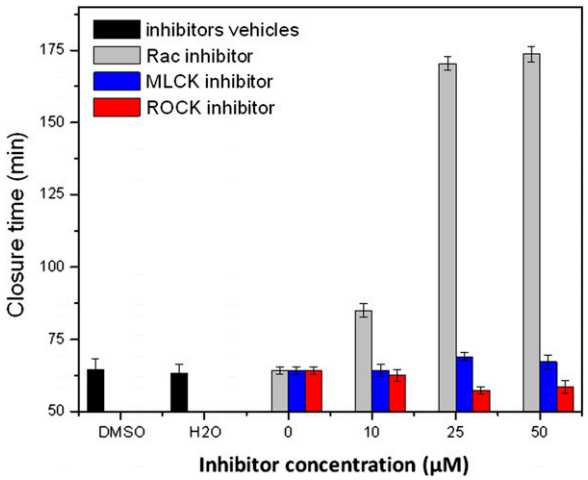

Fig. S6. Dose–inhibition response curve for the different inhibitors used (NSC23766, Y-27632, and ML-7) and their vehicles (either DMSO or water). The three concentrations tested are the most recurrently found in literature; 25 μM proved to be an adequate inhibitory concentration in our setup.

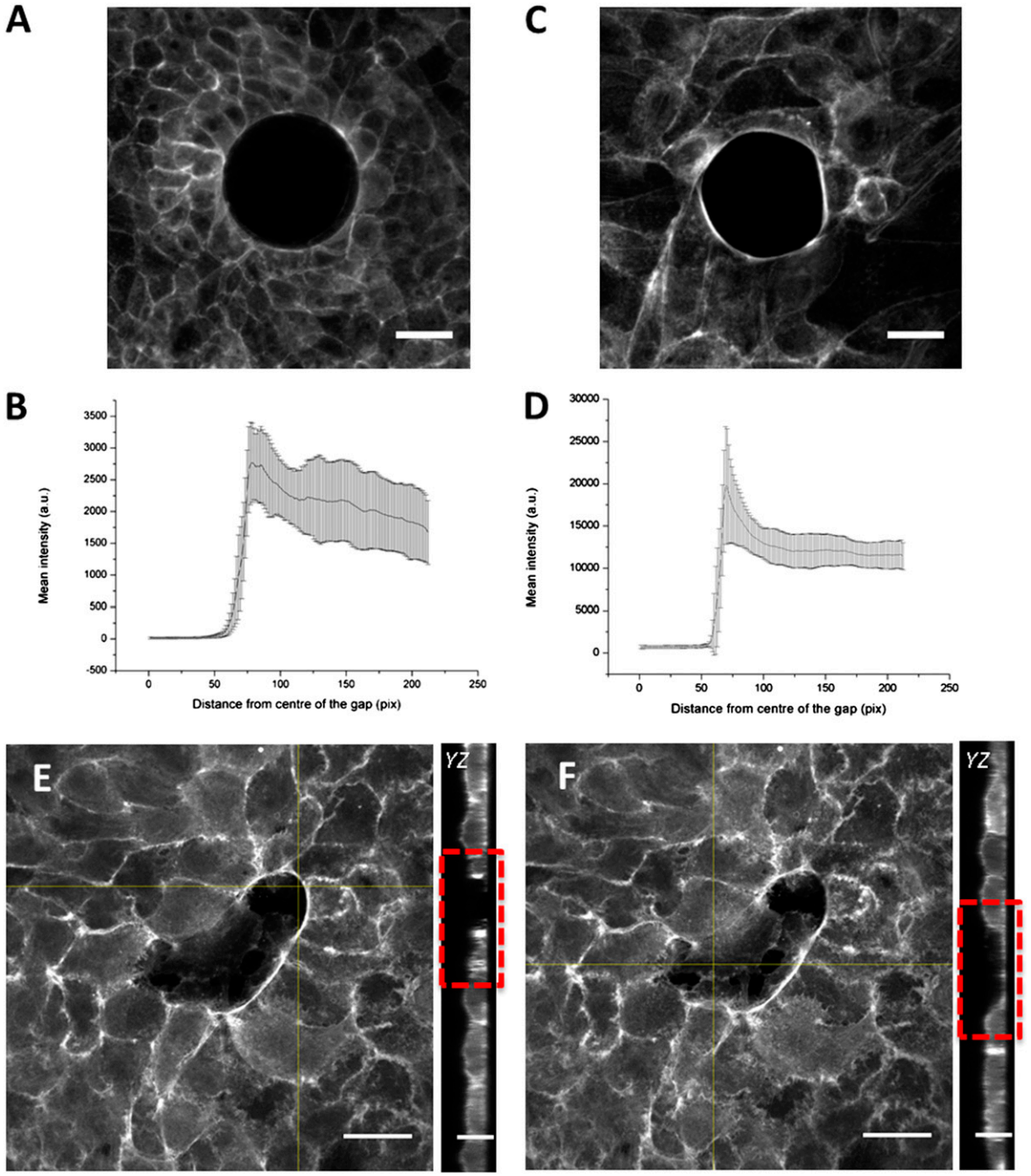

Fig. S7. Actin distribution showed by phalloidin staining. (*A*) Presence of the pillar does not promote accumulation of actin surrounding the pillar. (*B*) Quantification of actin fluorescence intensity in radial profiles (concentric circles of increasing diameter) at each given distance from the center of the gap. (*C*) Two minutes after releasing the pillar stencil, there is some actin clustering at the gap interface. (*D*) Peak of actin fluorescence intensity is more defined (higher and narrower). (*E* and *F*) Actin staining 30 min after pillar removal. As closure progresses, actin is still accumulated at the gap border where there are no lamellipodia (*E*) (see *y*–*z* orthogonal projection), whereas where the actin protrudes into the lamellipodia there is no actin clustering (*F*). (Scale bars, 20 μm.)

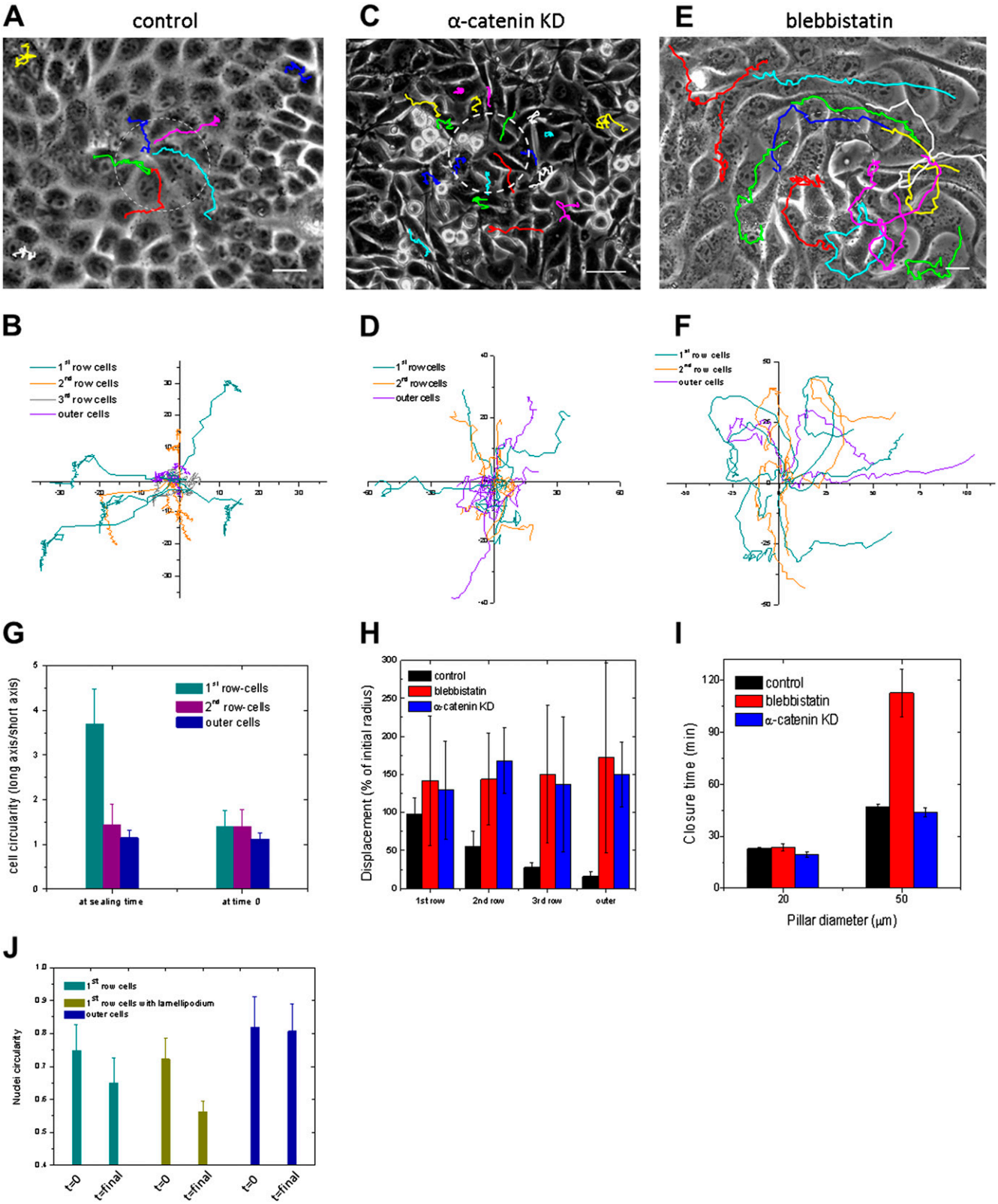

Fig. S8. Coordination of cells via cell–cell junctions and myosin action. (*A*–*F*) Trajectories of cells during the closure process. The tracks are shown after closure is completed. The dotted lines in the phase-contrast images represent the original gap margin. (*A*) Cell trajectories of control experiments. (Scale bar, 20 μm.) (*B*) Graph shows the trajectories (axis in micrometers) as a function of the cells' position with respect to the gap edge (i.e., first row corresponds to cells contacting the gap, second row refers to those behind, and consecutively). (*C* and *D*) α-Catenin knockdown MDCK cells during closure. (Scale bar, 20 μm.) (*E* and *F*) Blebbistatin-treated cells during closure. (Scale bar, 10 μm.) Trajectories from one experiment are shown, trends being representative of three other experiments analyzed. (*G*) Alignment of cells at the end of closure related to their initial shape, depending on their position with respect to the gap. (*H*) Dis-

Legend continued on following page

placement of cells indicated as a percentage of the initial radius of the gap, for control, α-catenin knockdown MDCK cells, and blebbistatin-treated cells, indicating the effective net movement of cells. (*I*) Closure time of 20- and 50-μm diameter gaps of α-catenin knockdown MDCK cells and cells treated with blebbistatin with respect to control conditions. For *G*, *H*, and *I*, data represent means and SEs of at least three experiments. (*J*) Changes in nuclei circularity during closure. Cells analyzed correspond to those contacting the gap (border cells), cells at the edge of the gap that extend lamellipodial during the closure, and cells far from the gap (outer cells) (typically taken at the four corners of the field of view).

Table S1. Comparison of the calculated area of the pillar used to pattern circular gaps with respect to the measured gap area right after pillar removal

Pillar diameter (μm)	Pillar area (μm^2)	Mean gap area (μm^2)	SD of gap area (μm^2)
15	177	163	33
20	314	327	15
30	707	727	30
40	1,257	1,311	58
50	1,963	1,965	14
60	2,827	2,826	11

Experimental data shown are means and SD of a minimum of seven experiments.

Table S2. Number of cells considered for the grouping on different degrees of cell density, always after reaching confluence

Normalized cell density	Cells/mm^2
<0.33	<1,200
0.33–0.46	1,200–1,700
0.46–0.6	1,700–2,200
0.6–0.8	2,200–3,000
0.8–1	3,000–3,700

Normalized cell density is obtained by dividing the number of cells per mm^2 by the maximal number of cells per mm^2. The bin labeled as <0.33 depicts low density, and the bin 1 is the mean of the three experiments at highest density. Data are mean and SD of at least three experiments each.

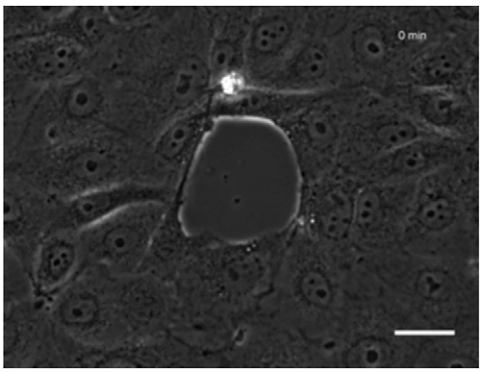

Movie S1. Video microscopy of gap closure. Note that lamellipodia are being extended by all of the cells contacting the gap. (Scale bar, 10 μm.)

Movie S1

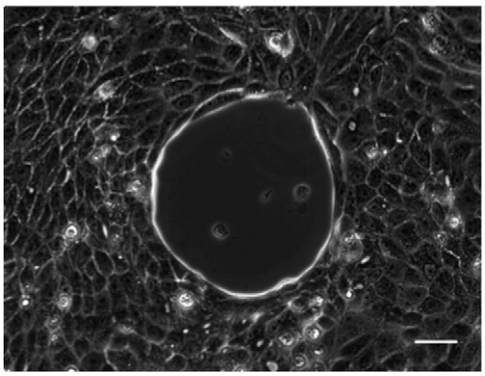

Movie S2. Video microscopy of a large gap closing. Note that broad lamellipodia are extended by cells surrounding the gap. (Scale bar, 20 μm.)

Movie S2

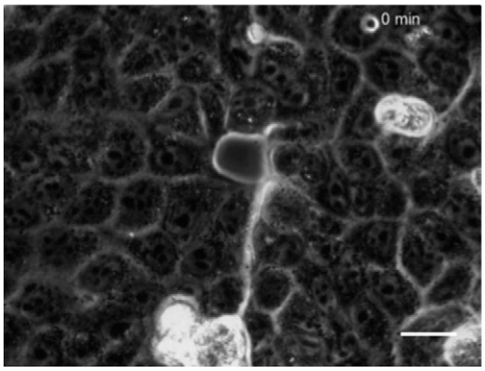

Movie S3. Video microscopy of gap closure on 1:40 PDMS cross-linking ratio substrate. Note that closure is impeded and gap acquires noncircular shapes. (Scale bar, 15 μm.)

Movie S3

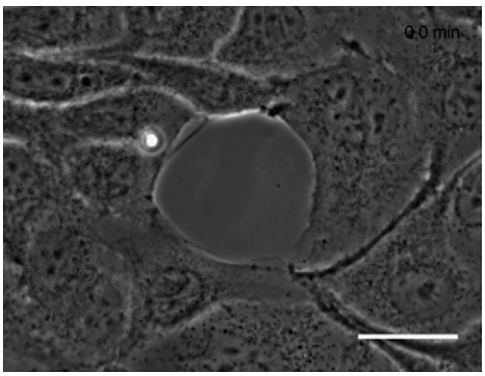

Movie S4. Video microscopy of gap closure under myosin light chain kinase inhibition by addition of 25 μM of ML-7. (Scale bar, 10 μm.)

Movie S4

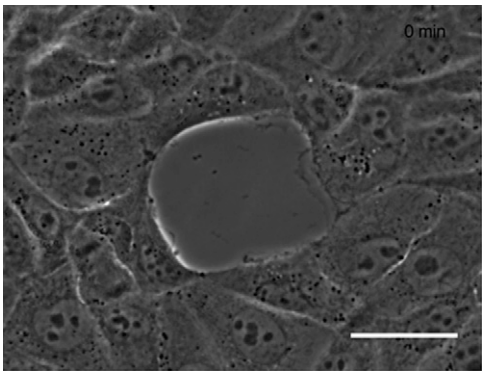

Movie S5. Video microscopy of gap closure under Rho kinase inhibition by addition of 25 μM of Y27632. (Scale bar, 15 μm.)

Movie S5

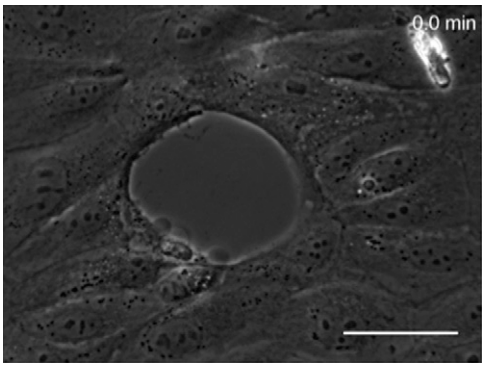

Movie S6. Video microscopy of gap closure under Rac1 inhibition by addition of 25 μM of NSC23766. (Scale bar, 10 μm.)

Movie S6

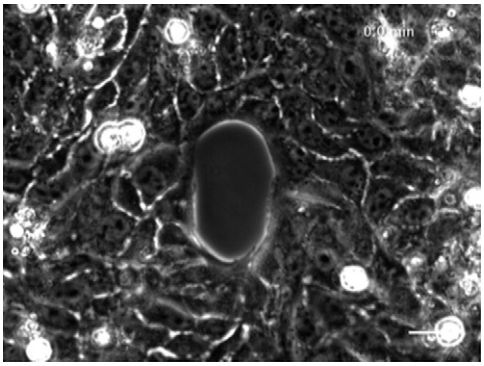

Movie S7. Video microscopy of an ellipsoidal gap closing. (Scale bar, 20 μm.)

Movie S7

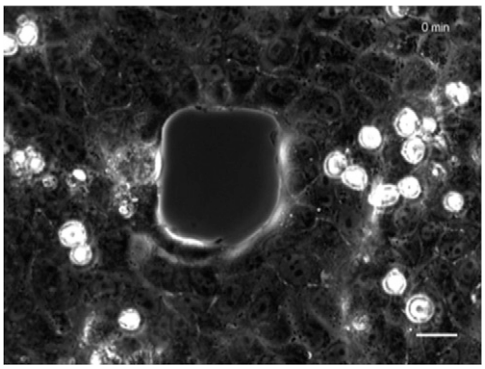

Movie S8. Video microscopy of a squared gap closing. (Scale bar, 20 μm.)

Movie S8

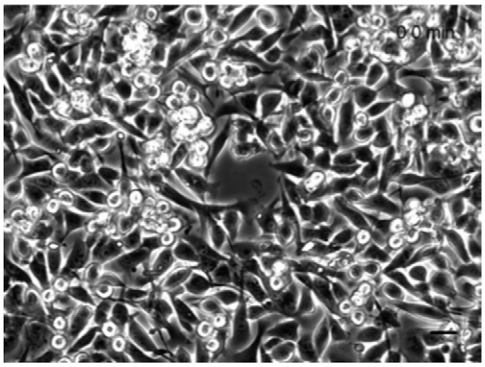

Movie S9. Video microscopy of gap closure with α-catenin knockdown MDCK cells. (Scale bar, 20 μm.)

Movie S9

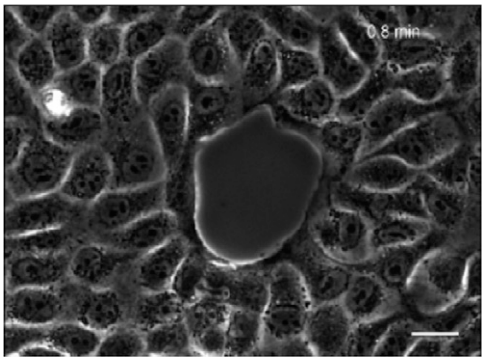

Movie S10. Video microscopy of a large gap closing under myosin inhibition by addition of 25 μM of blebbistatin. (Scale bar, 20 μm.)

Movie S10